ISSN 1547-4771, Physics of Particles and Nuclei Letters, 2022, Vol. 19, No. 3, pp. 196–201. © Pleiades Publishing, Ltd., 2022.

PHYSICS OF ELEMENTARY PARTICLES AND ATOMIC NUCLEI. THEORY

NLO QCD Corrections to Higgs Boson Production in Association with Gauge Bosons in Proton–Proton Collisions at $\sqrt{s} = 14$ TeV

K. Djamaa[a], * and A. Mohamed-Meziani[a], **

[a] *Department of Physics, Faculty of Exact Sciences, University of Bejaia, Bejaia, 06000 Algeria*

**e-mail: kenza.djamaa@univ-bejaia.dz*

***e-mail: abdelkader.mohamedmeziani@univ-bejaia.dz*

Received September 9, 2021; revised December 8, 2021; accepted December 13, 2021

Abstract—We suggest some predictions for Standard Model Higgs boson production in association with gauge bosons in proton-proton collisions at $\sqrt{s} = 14$ TeV. Our calculation includes the NLO QCD corrections of these processes using the MadGraph5_aMC@NLO event generator. We study the impact of these corrections on the total cross sections and on various kinematical distributions.

DOI: 10.1134/S1547477122030037

1. INTRODUCTION

The discovery of the Higgs boson at the LHC in 2012 [1, 2] was a watershed moment in high-energy physics. As a result, it is the source of the Standard Model's electroweak symmetry breaking mechanism and mass generation (SM). The Higgs boson production associated with gauge bosons W or Z (also known as the Higgs-strahlung process) is one of the most important Higgs production modes, it provides information about the Higgs boson couplings with the vector bosons and other SM particles, and it can be used to search for signals for Beyond Standard Model physics.

For these reasons, the ATLAS and CMS teams are very interested in the processes $pp \to VH$ ($V = W/Z$). The results of VH generation with the ATLAS detector were published in [3] for $\sqrt{s} = 7$ and 8 TeV center-of-mass energies. The ATLAS collaboration examined data acquired between 2015 and 2016 [4], and those between 2015 and 2018 [5] at $\sqrt{s} = 13$ TeV. The CMS experiment has given a search for studying VH generation at $\sqrt{s} = 8$ and 13 TeV, which correspond to integrated luminosities of 19.7 and up to 2.7 fb^{-1} respectively [6].

In recent years, a large number of theoretical predictions for H production associated with gauge bosons have been made, first at leading order only via $q\bar{q}$ [7, 8], then at next-to-leading order with QCD and EW corrections [9–12]. Computations of next-to-next-to-leading order QCD corrections to $pp \to VH$ were performed in [13]. The investigations of the off-shell of NLO for WH synthesis ($\text{H} \to b\bar{b}$, $W \to l\nu_l$) at $\sqrt{s} = 8$ and 14 TeV were performed using the MC@NLO simulation [14]. Tests of the relationship between a jet and WH production at $\sqrt{s} = 13$ TeV were accomplished with the NNLOJET framework and NNPDF31 from the LHAPDF library in [15]. The vh@nnlo software was used to compute ZH production at NNLO QCD corrections at $\sqrt{s} = 8$ and 14 TeV in [16]. The gluon-gluon and photon–photon collisions that lead to ZH formation were exposed in reference [17].

The VH production in proton–proton collisions at $\sqrt{s} = 14$ TeV is the subject of this research. These processes are carried out at LO and NLO using the MadGraph5 aMC@NLO [18] event generator. Numerical projections of their LO and NLO total cross sections, as well as the scale uncertainties associated with them are also presented. Using Pythia8 [19], we produce the different distributions of the gauge vector transverse momentum, the two tagging jets, and the missing transverse energy after the showering and the hadronisation.

The following is how the rest of the article is structured. In Section 2, we discuss the influence of the NLO QCD corrections on the contributions of VH production. We report our phenomenological findings on the total cross section and various distributions in Section 3. Finally, in Section 4, we provide our conclusions.

2. DETAILS OF THE CALCULATION

In this section, we focus on the production, on-shell, of the processes $pp \to VH$, where $V = W^{\pm}, Z$.

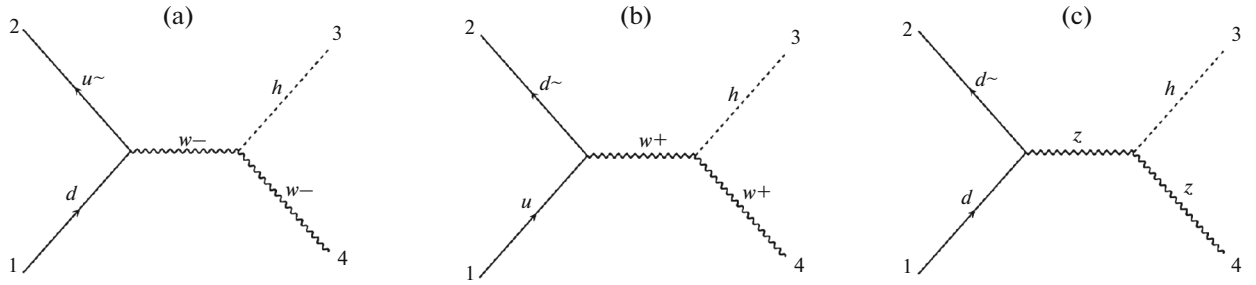

Fig. 1. Examples of Feynman diagrams for the different processes of VH production at tree-level.

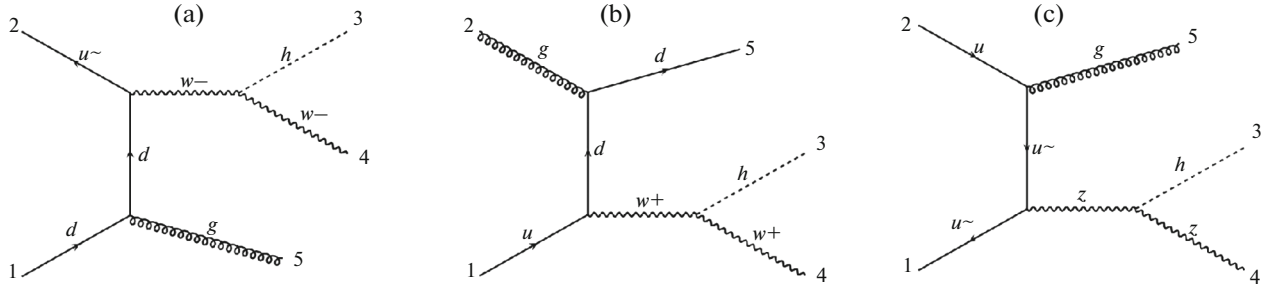

Fig. 2. Examples of Feynman diagrams of real corrections for the different processes of VH production.

We work in the context of the Standard Model with 4-flavour scheme, i.e. $p = u, d, c, s$ and gluons. We take into account the virtual bottom-loop, top-loop but not their contributions in the initial states. The collision events are generated at LO and NLO with QCD corrections using MadGraph5_aMC@NLO version 2.6.0.

We start by generating the processes at leading order, where the $pp \to W^{\pm}H$ processes are exclusively via the t-channel of $q\overline{q}'$ annihilation with exchange of $W^{\pm}$ bosons, as shown in Figs. 3a and 3b. However, the ZH production comes from the $q\overline{q}$ annihilation with exchange of the Z boson as displayed in Fig. 1c.

The $O(\alpha_s)$ NLO QCD corrections consist of new channels with a real and virtual contributions. They involve infrared (IR) and ultraviolet (UV) divergences that are regulated using the dimensional regularization (DR) scheme [20].

The real emission for VH production is essentially the tree-level diagrams with an additional parton and we classify it into two groups: $q\overline{q}' \to W^{\pm}H\ g$ and $q(\overline{q}')g \to W^{\pm}H\ q(\overline{q}')$ where some examples are given in Figs. 2a and 2b. The same is true for $pp \to ZH$ except that $q' = q$ as represented in Fig. 2c.

The virtual corrections are also computed. We noticed that the one-loops of $pp \to W^{\pm}H$ have triangle form and they are only obtained by $q\overline{q}'$ initiated as illustrated in Figs. 3a and 3b. While, those for ZH production are two types of loops, boxes and triangles, which are obtained by $q\overline{q}$ and gg contributions as shown in Fig. 3c. The gluon-initiated produces a top-quark and bottom loops which represent an interesting feature of the dominant contributions in the SM and beyond the SM.

3. PHENOMENOLOGICAL RESULTS AND DISCUSSION

In the following, we present our predictions of the total cross sections and kinematics variables distributions for VH production at LHC in the case of $\sqrt{s} =$ 14 TeV, using PYTHIA8 for showering and hadronization of the events. We employ NNPDF23 set parton distribution functions from LHAPDF setup [21], adopting the strong coupling constant $\alpha_s(M_Z) =$ 0.1137 and 0.1251 at LO and NLO respectively. Moreover, we take the central numerical value of the renormalization and factorization scales set to $\mu_R = \mu_F = M_H$.

For all the numerical results, we collect the following SM input parameters B :

$G_\mu = 1.16637 \times 10^{-5}$ GeV^{-2},	$\alpha^{-1} = 132.338$;
$M_W = 80.385$ GeV,	$\Gamma_w = 2.085$ GeV;
$M_Z = 91.188$ GeV,	$\Gamma_Z = 2.495$ GeV;
$M_H = 125$ GeV,	$\Gamma_H = 0.00407$ GeV;
$M_t = 173.2$ GeV,	$\Gamma_t = 1.4426$ GeV.

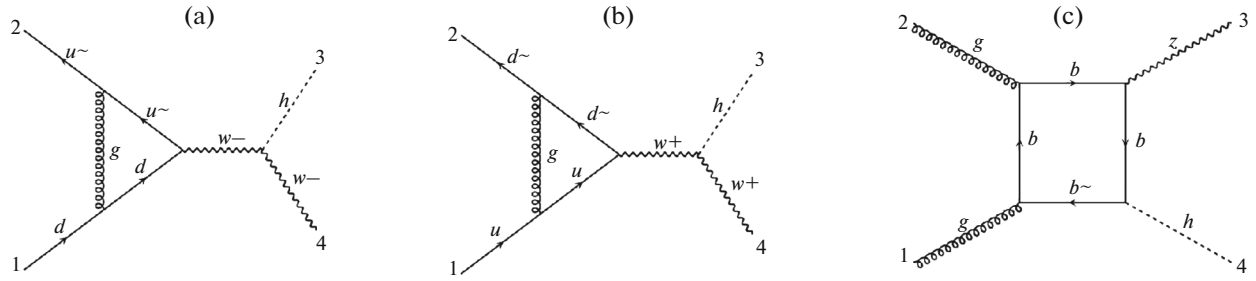

Fig. 3. Examples of Feynman diagrams of virtual corrections for the different processes of VH production.

Meanwhile, we impose the following cuts on transverse momentum, pseudo-rapidity of the leptons and jets:

$$\begin{aligned} &|\eta(l)| \le 2.5, \quad p_T(l) > 20 \text{ GeV}, \\ &|\eta(j)| \le 2.5, \quad p_T(j) > 10 \text{ GeV}. \end{aligned} \tag{1}$$

The jets are reconstructed with the anti-kT algorithm [22] with a radius parameter set to $R = 0.6$.

3.1. Total Cross Sections

In Table 1, we report the results of our predictions of the LO and NLO total cross sections and their corresponding K-factors for VH production. The impact of the NLO QCD corrections ranges from 32 to 38% of the LO term for all our processes. This is due to the real and the virtual contributions introduced at NLO. We remind that the ZH production via the $gg \to ZH$ process contributes only at next-to-leading order (NLO) and that its cross section is: $\sigma_{\text{NLO}}^{gg\to ZH} = 0.066 \pm 2.8\times10^{-4}{}^{+24.3\%}_{-18.6\%}$ which represents 7% of the total cross section. Table also shows that the size of the QCD corrections is large for the $pp \to W^-H$ process with the largest value of the K factor equal to 1.38.

Our predictions of the total cross sections are in good agreement with those presented in [23] at 13 TeV. The same is true when we compare them with experimental measurements given by the ATLAS Collaboration [4] in pp collisions at $\sqrt{s} = 13$ TeV using the data collected during 2015 and 2016:

$$\sigma_{WH}\mathcal{B}_{H\to WW^*} = 0.67^{+0.31}_{-0.27}\,(\text{stat.})^{+0.14}_{-0.11}(\text{exp syst.})^{+0.11}_{-0.09}\,(\text{theo syst.})\ \text{pb},$$

$$\sigma_{ZH}\mathcal{B}_{H\to WW^*} = 0.54^{+0.31}_{-0.24}\,(\text{stat.})^{+0.10}_{-0.05}(\text{exp syst.})^{+0.11}_{-0.05}(\text{theo syst.})\ \text{pb}.$$

with $\mathcal{B}_{H\to WW^*}$ is the branching-fraction values.

In the same table, we have estimated the theoretical errors come with our calculations. The first ones are deposited directly after the values of the total cross sections, they are the statical errors of the Monte Carlo simulations and the next ones are the scale uncertainties, simulated by varying simultaneously μ_R and μ_F between $0.5M_H < \mu_R, \mu_F < 2M_H$ with the constraint $0.5 < \mu_R/\mu_F < 2$. We note that the scale uncertainties at NLO are smaller than the corresponding ones of the LO results.

3.2. Distributions

Now, we investigate various kinematical distributions, we recall that all these distributions are normalized to one.

We begin with the transverse moments of the vector bosons at partonic level, as plotted in Fig. 4. We see that the LO and NLO distributions have the same shape for all $pp \to VH$ processes ($V = W^{\pm}$ and Z). We

Table 1. The LO and NLO total cross section of VH production at $\sqrt{s} = 14$ TeV

	σ_{LO}, pb	σ_{NLO}, pb	$K = \dfrac{\sigma_{\text{NLO}}}{\sigma_{\text{LO}}}$
W^-H	$0.44 \pm 5.2\times10^{-4}{}^{+3.58\%}_{-4.37\%}$	$0.605 \pm 1.5\times10^{-3}{}^{+1.7\%}_{-2.3\%}$	1.38
W^+H	$0.717 \pm 5.3\times10^{-4}{}^{+3.22\%}_{-3.95\%}$	$0.947 \pm 2.4\times10^{-3}{}^{+2.2\%}_{-2.6\%}$	1.32
ZH	$0.608 \pm 5.9\times10^{-4}{}^{+3.11\%}_{-3.85\%}$	$0.887 \pm 1.4\times10^{-3}{}^{+2.0\%}_{-2.4\%}$	1.35

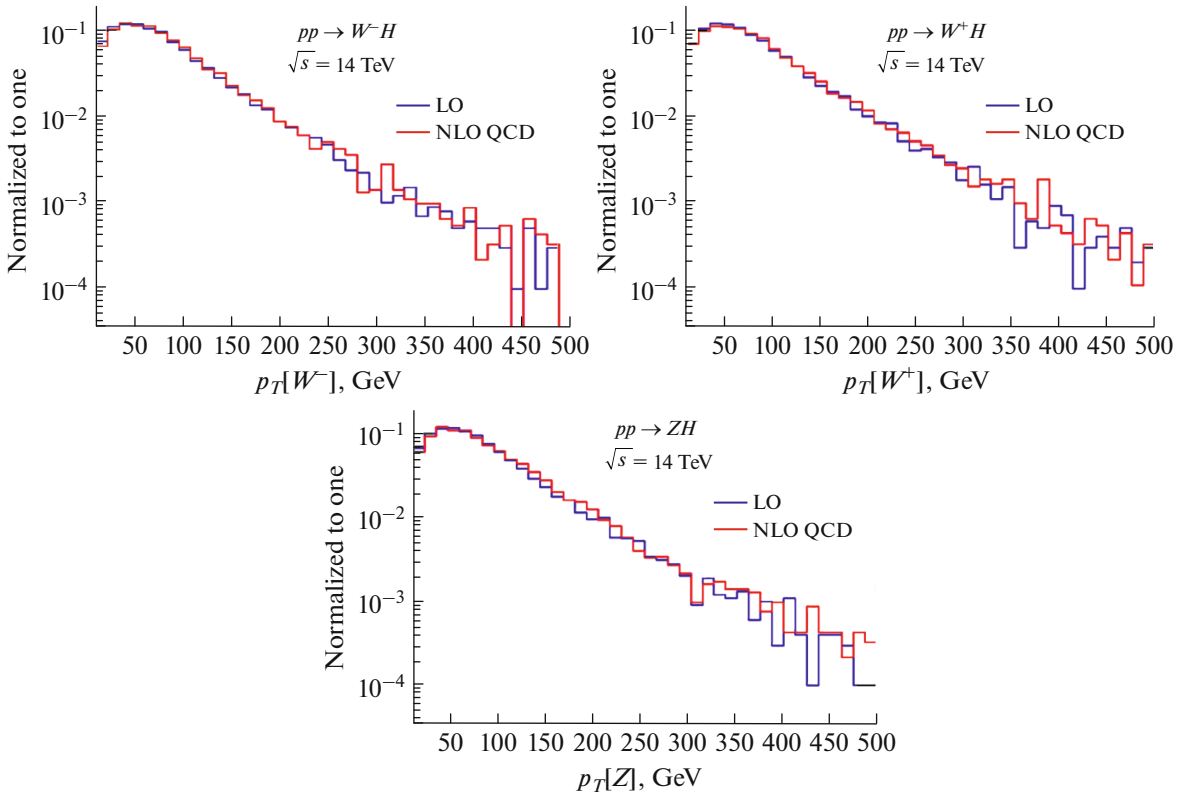

Fig. 4. The LO and NLO transverse momentum distributions of vector bosons for VH productions at $\sqrt{s} = 14$ TeV.

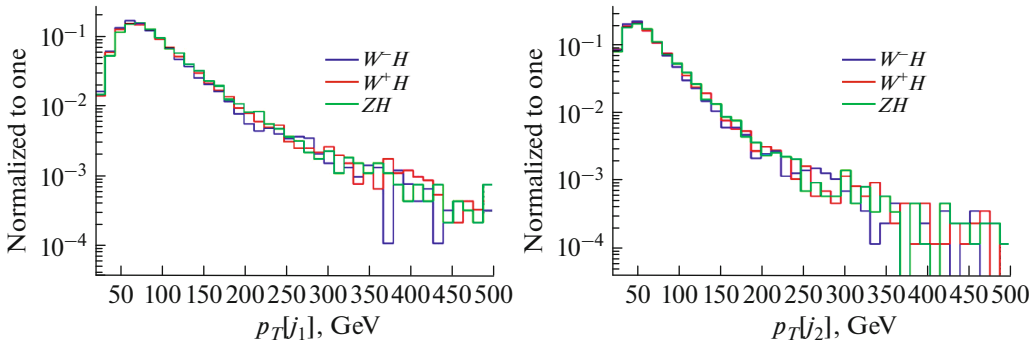

Fig. 5. Transverse momentum distributions of the two tagging jets reconstructed at NLO-QCD for VH productions at $\sqrt{s} = 14$ TeV.

can distinguish also two regions; the first one corresponds to where the distributions grow lightly, at low values of the transverse momentums $p_T(V) < 60$ GeV, and the second to the region where the distribution decreases for the rest $p_T(V)$.

The transverse momentum distributions of the two tagging jets reconstructed at NLO-QCD and ΔR distance (a separation between two hardest jets) are reported in Figs. 5 and 6, respectively.

The behaviour of the hardest jets distributions has globally similar appearance for all processes, indeed at low $p_T(j_1) < 80$ GeV and $p_T(j_2) < 50$ GeV, the distributions are the largest, then they increase slightly. The next-to-hardest jet distribution vanishes rapidly comparing to the leading jet one. Additionally, the peaks of the ΔR distributions are around 3.

Figure 7 shows the E_T^{miss} distributions for the W^+H, W^-H and ZH processes. These distributions have the

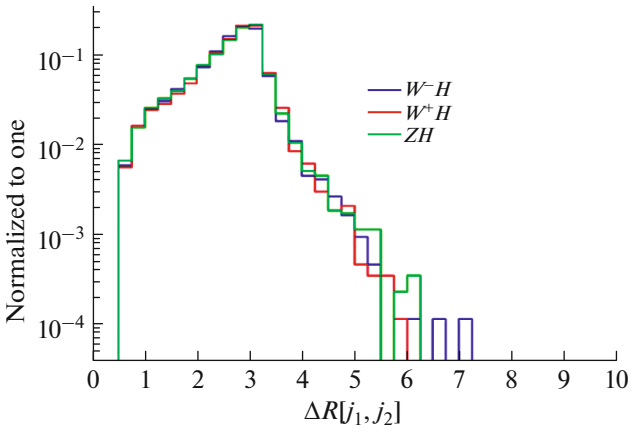

Fig. 6. The corresponding separation ΔR distributions for VH productions at $\sqrt{s} = 14$ TeV.

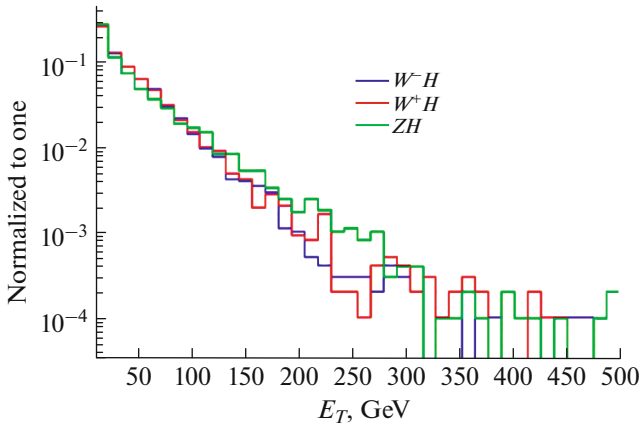

Fig. 7. Missing energy transverse distributions for VH productions at $\sqrt{s} = 14$ TeV.

same behaviour. Indeed, the distributions decrease with the increment of E_T^{miss}. From $E_T^{\text{miss}} > 150$ GeV, the signal for ZH production is greater than that for $W^{\pm}H$, this is due to the top-quark-loop included by the gg fusion.

4. CONCLUSIONS

We have simulated the production of the Higgs boson associated with the vector bosons $W^{\pm}$ and Z in proton-proton collisions at $\sqrt{s} = 14$ TeV. We have illustrated the effects of NLO QCD corrections on this production. The latter produce new channels like gluon-gluon fusion which appears only at this level for the ZH production. The NLO QCD corrections also affect on the calculation of the total cross sections and we found that these corrections are of the order of 38% of the first term. The scale uncertainties have equally been estimated, they vary from −4.37 to +3.58%.

We have shown the shape of the spectrum for transverse momentum of vector bosons at parton level, that are similar for all $pp \to VH$ processes ($W^{\pm}$, Z). The transverse momentum of the two tagging jets reconstructed at the first perturbative order allows us to confirm that the distribution is more sizeable at $p_T(j_1) < \mathrm{M}_{V+H}$. For all VH production processes, the maximum of the separation distance between two hardest jets is at $\Delta R = 3$. We finally have pointed out the behaviour of the transverse missing energy. These distributions have the same behaviour, they decrease with the increment of E_T^{miss}. Because of the gg fusion, the signal for ZH production has the greatest E_T^{miss} that the other signals, W^+H and W^-H.

We conclude that this study is an interesting analysis and that we can expand it in different channels as $H \to b\bar{b}$ and exploit the information in new physics searches, We leave this for investigate in the near future.

ACKNOWLEDGMENTS

This work was realized with the support of the Algerian Ministry of Higher Education and Scientic Research.

CONFLICT OF INTEREST

The authors declare that they have no conflicts of interest.

REFERENCES

1. The ATLAS Collab., "Observation of a new particle in the search for the standard model Higgs boson with the ATLAS detector at the LHC," Phys. Lett. B **716**, 1–29 (2012); arXiv: 1207.7214 [hep-ex].
2. The CMS Collab., "Observation of a new boson at a mass of 125 GeV with the CMS experiment at the LHC," Phys. Lett. B **716**, 30 (2012); arXiv: 1207.7235 [hep-ex].
3. The ATLAS Collab., "Study of (W/Z)H production and Higgs boson couplings using $H \to WW^*$ decays with the ATLAS detector," J. High Energy Phys. **08**, 137 (2015); arXiv: 1506.06641 [hep-ex].
4. The ATLAS Collab., "Measurement of the production cross section for a Higgs boson in association with a vector boson in the $H \to WW^* \to l\nu l\nu$ channel in pp collisions at $\sqrt{s} = 13$ TeV with the ATLAS detector," Phys. Lett. B **798**, 134949 (2019); arXiv: 1903.10052 [hep-ex].
5. The ATLAS Collab., "Measurements of WH and ZH production in the $H \to b\bar{b}$ decay channel in p p collisions at 13TeV with the ATLAS detector," Eur. Phys. J. C **81**, 178 (2021); arXiv: 2007.02873 [hep-ex].

6. The CMS Collab., "Combination of searches for heavy resonances decaying to WW, WZ, ZZ, WH, and ZH boson pairs in proton-proton collisions at $\sqrt{s} = 8$ and 13 TeV," Phys. Lett. B **774**, 533 (2017); arXiv: 1705.09171 [hep-ex].
7. C. Zecher, T. Matsuura, and J. J. van der Bij, "Leptonic signals from off-shell Z boson pairs at hadron colliders," Z. Phys. C **64**, 219–226 (1994); arXiv: 9404295 [hep-ph].
8. Q. Hong Cao, C. Sheng Li, and S. Hua Zhu, "Leading electroweak corrections to the neutral Higgs boson production at the Fermilab tevatron," Commun. Theor. Phys. **33**, 275–284 (2000); arXiv: 9810458 [hep-ph].
9. H. Baer, B. Bailey, and J. F. Owens, "$O(\alpha_s)$ Monte Carlo approach to W^+ Higgs associated production at hadron supercolliders," Phys. Rev. D **47**, 2730 (1993).
10. A. Banfi and J. Cancinob, "Implications of QCD radiative corrections on high-pT Higgs searches," Phys. Lett. B **718**, 499–506 (2012); arXiv: 1207.0674 [hep-ph].
11. T. Han and S. Willenbrock, "QCD correction to the $pp \to WH$ and ZH total cross sections," Phys. Lett. B **273**, 167–172 (1991).
12. M. L. Ciccolini, S. Dittmaier, and M. Kramer, "Electroweak radiative corrections to associated WH and ZH production at hadron colliders," Phys. Rev. D **68**, 073003 (2003); arXiv: 0306234 [hep-ph].
13. O. Brein, A. Djouadi, and R. Harlander, "NNLO QCD corrections to the Higgs-strahlung processes at hadron colliders," Phys. Lett. B **579**, 149–156 (2004); arXiv: 0307206 [hep-ph].
14. G. Ferrera, M. Grazzini, and F. Tramontano, "Higher-order QCD effects for associated WH production and decay at the LHC," J. High Energy Phys. **2014**, 39 (2014); arXiv: 1312.1669 [hep-ph].
15. R. Gauld, A. Gehrmann-de Ridder, E. W. N. Glover, A. Huss, and I. Majer, "Precise predictions for WH^+ jet production at the LHC," arXiv: 2009.14209 [hep-ph] (2020).
16. G. Ferrera, M. Grazzini, and F. Tramontano, "Associated ZH production at hadron colliders: The fully differential NNLO QCD calculation," Phys. Lett. B (2014); arXiv: 1407.4747 [hep-ph].
17. F. M. Renard, "Test of Higgs boson compositeness in ZH production through gluon-gluon and photon-photon collisions," arXiv: 1701.09116 [hep-ph] (2017).
18. J. Alwall, M. Herquet, F. Maltoni, O. Mattelaerc, and T. Stelzerd, "MadGraph 5: Going beyond," J. High Energy Phys. **2011**, 128 (2011); arXiv: 1106.0522 [hep-ph].
19. T. Sjostrand, S. Mrenna, and P. Z. Skands, "A brief introduction to PYTHIA 8.1," Comput. Phys. Commun. **178**, 852–86 (2007); arXiv:0710.3820 [hep-ph].
20. G. 't Hooft and M. Veltman, "Regularization and renormalization of Gauge fields," Nucl. Phys. B **44**, 189–213 (1972).
21. The NNPDF Collab., "Parton distributions with LHC data," Nucl. Phys. B (2012); arXiv: 1207.1303 [hep-ph].
22. M. Cacciari, G. P. Salam, and G. Soyez, "The anti-Kt jet clustering algorithm," J. High Energy Phys. **04**, 063 (2008); arXiv:1111.6097 [hep-ph].
23. J. Alwall, R. Frederix, S. Frixione, V. Hirschi, F. Maltoni, O. Mattelaer, H.-S. Shao, T. Stelzer, P. Torrielli, and M. Zaro, "The automated computation of tree-level and next-to-leading order differential cross sections, and their matching to parton shower simulations," J. High Energy Phys. **07**, 079 (2014); arXiv: 1405.0301 [hep-ph].